RESULTS ON HEAVY-ION PHYSICS WITH THE CMS DETECTOR AT THE LHC*

Bożena Boimska

on behalf of the CMS Collaboration

National Centre for Nuclear Research
Hoża 69, 00-681, Warszawa, Poland

(Received April 29, 2013)

Selected experimental results related to heavy-ion physics, obtained using the Compact Muon Solenoid (CMS) detector at the Large Hadron Collider (LHC), are presented. Measurements have been performed for lead–lead (PbPb), proton–lead (pPb) and proton–proton (pp) data samples collected in the years 2010–2012. The jet-quenching phenomenon has been studied by looking at the production of the so-called "hard probes", such as high transverse momentum charged particles, isolated photons, Z and W bosons, and jets. In addition, the suppression of quarkonium states and long-range two-particle correlations have been investigated.

DOI:10.5506/APhysPolB.44.1363
PACS numbers: 25.75.–q, 13.85.–t

1. Introduction

The theory of strong interactions — Quantum Chromodynamics (QCD) — predicts that at the extremely high energy density of about 1 GeV/fm^3 and temperature of 150–190 MeV, nuclear matter undergoes a phase transition to a state of deconfined quarks and gluons. This state is called Quark-Gluon Plasma (QGP) and is studied experimentally by colliding heavy ions, such as Pb nuclei, at relativistic energies.

Heavy-ion collisions at the LHC accelerator allow to study QCD in unexplored, so far, kinematic domain and to investigate the influence of the hot, colored, high-density matter created in the collision on particle production. The CMS experiment at the LHC is dedicated to studies of pp interactions but it is also excellent for heavy-ion measurements. It is well

* Presented at the Cracow Epiphany Conference on the Physics After the First Phase of the LHC, Kraków, Poland, January 7–9, 2013.

suited for investigating the bulk particle production, collective phenomena and, in particular, for studying various hard probes. Main parts of the CMS apparatus are the tracking system, calorimeters and muon system, which are covering a wide pseudorapidity[1] range. The high-precision silicon tracking system is located in the 3.8 T field of the superconducting solenoid. It measures charged particles within the pseudorapidity range $|\eta| < 2.5$ and consists of silicon pixel and silicon strip detector modules. The electromagnetic (ECAL) and hadronic (HCAL) calorimeters are also located inside the solenoid. The ECAL consists of lead-tungstate crystals, arranged in a quasi-projective geometry and distributed in a barrel region ($|\eta| < 1.5$) and two endcaps that extend up to $|\eta| = 3.0$. The HCAL barrel and endcaps are sampling calorimeters composed of brass and scintillator plates, covering $|\eta| < 3.0$. Iron hadronic forward calorimeters (HF) with quartz fibers, read out by photomultipliers, extend the calorimeter coverage up to $|\eta| = 5.2$. Muons are measured within $|\eta| < 2.4$ in gas-ionization detectors, which are embedded in the steel return yoke. The subdetectors are complemented by a flexible two-level trigger system. A detailed description of the CMS detector can be found elsewhere [1].

High center-of-mass energies of collisions happening at the LHC and the excellent features of the CMS detector allow to measure some signals/observables for the first time. A few such measurements are presented and discussed in this conference report. In general, the results shown pertain to the jet-quenching phenomenon, suppression of quarkonium states and the so-called "ridge effect", which is studied in two-particle correlations. The observables were analyzed in bins of the collision centrality. Centrality can be specified by giving a percentage of the total inelastic cross section. The number of participating nucleons, N_{part}, and the number of binary nucleon–nucleon collisions, N_{coll}, are also used as measures of centrality. In order to obtain N_{part} and N_{coll} values, the energy measured in HF calorimeters (or event multiplicity from the silicon tracker) is compared to simulations including the Glauber model calculations and response of the detectors.

Analyzes described in this paper are based on data samples recorded in the years 2010–2012. In 2010 and 2011, CMS collected samples of PbPb collisions at a nucleon–nucleon center-of-mass energy $\sqrt{s_{NN}} = 2.76$ TeV, corresponding to integrated luminosities of about 7 and 150 $\mu\mathrm{b}^{-1}$, respectively. In addition, reference pp data at the same collision energy were also taken in 2011 — recorded integrated luminosity of 231 nb^{-1}. A short pilot run in September 2012, lasting for about 8 hours, for pPb collisions at $\sqrt{s_{NN}} = 5.02$ TeV resulted in the integrated luminosity of about 1 $\mu\mathrm{b}^{-1}$.

[1] Pseudorapidity η is defined as $\eta = -\ln(\tan(\theta/2))$, where θ is the polar angle of the particle with respect to the anti-clockwise beam direction.

2. Selected PbPb results

2.1. Jet quenching

One of the signatures for the formation of a deconfined system of quarks and gluons (QGP) in high-energy heavy-ion collisions is the jet-quenching effect [2]. It has been predicted that interactions of highly energetic partons with a hot and dense colored matter, created in the collision, would induce a gluon radiation which carries off a significant fraction of the parton's energy, thus leading to the depletion of jet yields at high transverse momenta (p_{T}). First, indirect measurements of energy loss in the medium were performed at the Relativistic Heavy Ion Collider (RHIC), by studying yields and correlations of high-p_{T} particles that originate from jet fragmentation [3, 4]. At LHC energies, jet quenching can be investigated not only for particles at even higher transverse momenta than at RHIC but also directly for fully reconstructed jets.

Results presented below were obtained for the so-called "hard probes" — particles or jets produced in hard processes — characterized by a large energy or mass. Hard probes are well calibrated, as their expected yields can be calculated in the perturbative QCD theoretical framework. They fall into two categories: strongly-interacting probes (*e.g.* hadrons and jets) — thus expected to be modified by the medium, and probes which do not interact strongly (*e.g.* high-energy prompt photons and weak bosons). The latter serve as reference probes.

Nuclear modification factor

One of the key observables in studies of jet quenching is the nuclear modification factor

$$R_{AA}(p_{\mathrm{T}}) = \frac{1}{T_{AA}} \frac{d^2N^{AA}/dp_{\mathrm{T}}d\eta}{d^2\sigma^{NN}/dp_{\mathrm{T}}d\eta}\,, \tag{1}$$

where the nuclear overlap function $T_{AA} = \langle N_{\mathrm{coll}} \rangle / \sigma_{\mathrm{inel}}^{NN}$ can be calculated from the Glauber model accounting for the nuclear collision geometry. The nuclear modification factor is defined as the ratio of particle yields in nucleus–nucleus (AA) compared to nucleon–nucleon (NN) collisions, normalized by T_{AA}. The jet-quenching effect is observed at high-p_{T} when $R_{AA} < 1$ — so, the production of particles is suppressed in AA collisions.

CMS has obtained R_{AA} for various particles as well as jets, see Fig. 1. Bosons mediating electroweak interactions (photon, W and Z) play an important role as reference signals for strongly-interacting probes. Prompt photons, produced via quark–gluon Compton scattering or quark–antiquark annihilation, are separated from the photons arising from parton fragmentation processes (mainly π^0, η decays) by applying isolation criteria in the

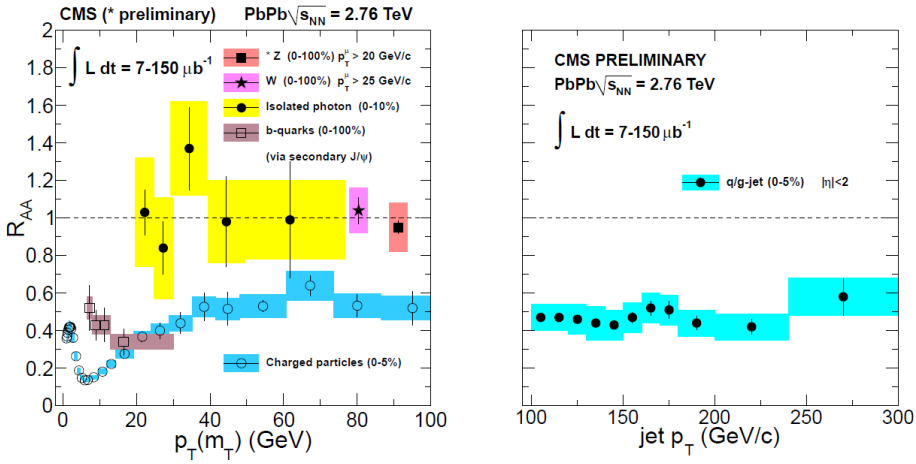

Fig. 1. Nuclear modification factors for isolated photons [5], Z [6] and W [7] bosons, charged particles [8] and b-quarks measured by separating secondary J/ψ particles [9] (left), and reconstructed jets [10] (right). For Z and W, data points are plotted at the rest mass of particles. For charged hadrons, the pion mass is assumed. Photons, charged hadrons and jets are detected in central collisions.

tracker, electromagnetic and hadronic calorimeters, followed by shower shape criteria in the highly segmented electromagnetic calorimeter. In PbPb collisions, the normalized yield of these isolated photons at high p_{T} [5] as well as yields of $Z \to \mu^+\mu^-$ [6] and $W \to \mu\nu$ [7] are consistent with those measured in pp interactions at the same center-of-mass energy, leading thus to $R_{AA} = 1$ (left panel of Fig. 1).

For charged hadrons, in contrast to previously mentioned bosons, in central PbPb collisions values $R_{AA} < 1$ are observed [8], as shown in the left panel in Fig. 1. Values $R_{AA} < 1$ were obtained also for b-quarks in the recent CMS analysis of non-prompt J/ψ originating from decays of B mesons [9]. Both measurements are in agreement with the presence of jet quenching in PbPb collisions at the LHC.

The right panel in Fig. 1 presents first, preliminary results on the nuclear modification factor for fully reconstructed jets. For the 5% most central PbPb collisions, the suppression of jet yield by a factor of about two was measured [10]. The jet R_{AA} is approximately flat as a function of p_{T}, over the p_{T} range studied. The similarity of R_{AA} factors obtained for jets in the 100–200 GeV/c range and for charged particles in the 50–100 GeV/c range is apparent. It can be explained by taking into account the fact that, typically, leading charged particles originate from the fragmentation of jets with about two times larger transverse momentum.

Jet–jet events

Using fully reconstructed jets, the parton energy loss can be studied more directly, bypassing complications of the jet fragmentation process. In the absence of medium effects, jets in dijet events should have transverse momenta of similar magnitude and be emitted back-to-back. For the case of parton energy losses in the medium, the dijet event characteristics may change, *e.g.* p_{T} of jets can be modified.

To characterize the dijet transverse momentum imbalance quantitatively, an asymmetry ratio is defined

$$A_J = \frac{p_{\mathrm{T},1} - p_{\mathrm{T},2}}{p_{\mathrm{T},1} + p_{\mathrm{T},2}}\,, \tag{2}$$

where $p_{\mathrm{T},1}$ is the transverse momentum of the "leading" jet, and $p_{\mathrm{T},2}$ is the momentum of the "subleading" jet.

The centrality dependence of dijet asymmetry in PbPb collisions is shown in Fig. 2 [11]. A_J was calculated for pairs of jets for which the leading jet $p_{\mathrm{T},1} > 120$ GeV/c and the subleading jet $p_{\mathrm{T},2} > 30$ GeV/c selections were

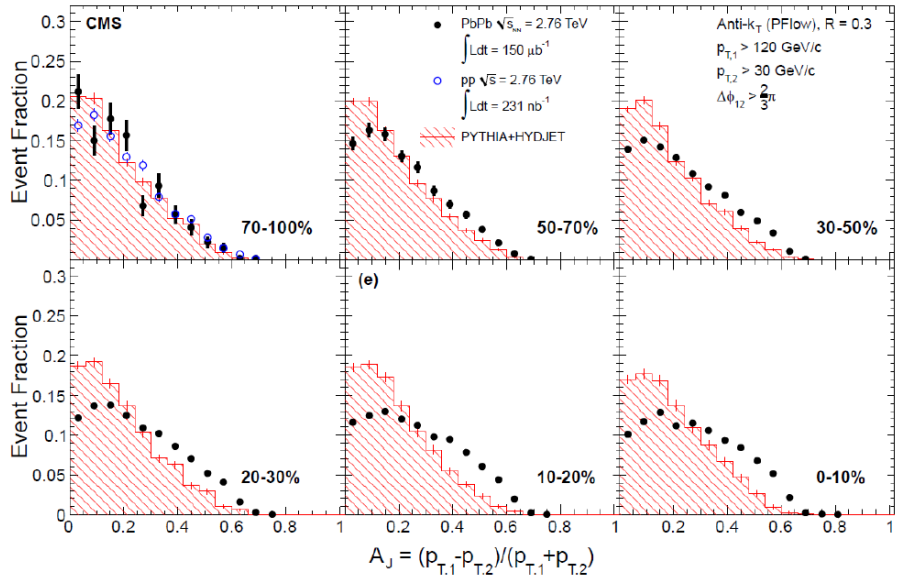

Fig. 2. Dijet asymmetry ratio (A_J) for leading jets of $p_{\mathrm{T},1} > 120$ GeV/c and subleading jets of $p_{\mathrm{T},2} > 30$ GeV/c, separated in azimuthal angle by $\Delta\phi_{12} > 2\pi/3$ [11]. The jets are restricted to $|\eta| < 2$. A_J distributions are shown for different centrality classes. PbPb data are presented as solid points. For the most peripheral collisions (70–100%), the distribution from *pp* collisions (circles) is superimposed. Simulations of PYTHIA dijets embedded into HYDJET PbPb collisions (hatched areas) are shown for comparison.

used. In addition, to ensure that dijets are approximately back-to-back, a cut $\Delta\phi_{12} > 2\pi/3$ was applied. For the most peripheral PbPb collisions, the A_J distribution is in good agreement with the *pp* data and the reference distribution (PYTHIA+HYDJET). The dijet momentum imbalance increases with centrality and is the largest for the (0–10%) most central collisions — the imbalance for PbPb is significantly larger than that for the reference distribution. This observation is consistent with the jet-quenching scenario, in which partons lose their energy traversing the hot and dense QCD medium. On the other hand, the distribution of the azimuthal angle difference between the two jets, $\Delta\phi_{12}$, remains sharply peaked at 180 degrees [12]. This leads to the conclusion that the parton energy loss does not cause a visible angular decorrelation and rules out single-hard-gluon radiation as the main energy loss mechanism.

Photon–jet events

Recently, a further evidence for the parton energy loss was presented in the form of momentum imbalance in γ-jet correlations [13]. As shown earlier, high-energy photons are not modified by the presence of strongly interacting medium (R_{AA} =1) and may serve as an energy tag for the jet partner in photon–jet events. The p_{T}-momentum imbalance can be quantified by the ratio $X_{J\gamma} = p_{\mathrm{T}}^{\mathrm{jet}}/p_{\mathrm{T}}^{\gamma}$. Its mean value, $\langle X_{J\gamma}\rangle$, is presented in

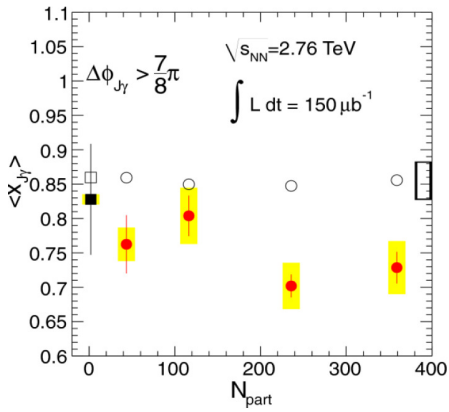

Fig. 3. (Color online) Mean values of the jet-to-photon p_{T} ratio as a function of the number of participant nucleons, for isolated photons of $p_{\mathrm{T}}^{\gamma} > 60$ GeV/c and jets of $p_{\mathrm{T}}^{\mathrm{jet}} > 30$ GeV/c [13]. Photons were restricted to the region of $|\eta| < 1.44$ and jets to $|\eta| < 1.6$. PbPb data are shown as red solid points, and PYTHIA+HYDJET simulations as circles. Results for *pp* data (black filled square) and PYTHIA-*pp* (open square) are also presented. Error bars and yellow boxes denote statistical and point-to-point systematic uncertainties, respectively. The empty box at the far right indicates the correlated systematic uncertainty.

Fig. 3 as a function of collision centrality — defined by the number of nucleons participating in the PbPb collision (N_{part}). The jet-to-photon ratio of transverse momenta is reduced in PbPb collisions with respect to pp collisions and with respect to the reference PYTHIA+HYDJET simulations. For the specific thresholds of the analysis, $p_{\mathrm{T}}^{\gamma} > 60$ GeV/c and $p_{\mathrm{T}}^{\mathrm{jet}} > 30$ GeV/c, this reduction is of the order of 15% for central collisions. This observation is yet another manifestation of jet quenching. Similarly as for jet–jet events, the jet and the photon are approximately back-to-back in azimuthal angle [13].

Missing transverse momentum

The analysis of jet–jet and photon–jet events has shown the presence of p_{T} imbalance. One may ask: how is the missing transverse momentum redistributed? In order to answer this question, the projection of missing p_{T} of reconstructed charged tracks onto the leading jet axis, $\not{p}_{\mathrm{T}}^{||}$, was studied for dijet events [12]. For each event, this projection was calculated as

$$\not{p}_{\mathrm{T}}^{||} = \sum_{i} -p_{\mathrm{T}}^{i} \cos\left(\phi_i - \phi_{\text{Leading Jet}}\right), \tag{3}$$

where the sum goes over all tracks with $p_{\mathrm{T}} > 0.5$ GeV/c and $|\eta| < 2.4$. The results were then averaged over all events to obtain $\left\langle \not{p}_{\mathrm{T}}^{||} \right\rangle$. Negative values of $\left\langle \not{p}_{\mathrm{T}}^{||} \right\rangle$ correspond to the excess towards the leading jet, and positive ones to the excess in the direction of the subleading jet.

The average missing transverse momentum as a function of dijet asymmetry (A_J), for the 0–30% central collisions, is shown in Fig. 4. Contributions to the missing transverse momentum from various ranges of track p_{T} are presented as colored bands. Taking into account all charged particles in the events (left panel of Fig. 4) the momentum balance is restored, $\left\langle \not{p}_{\mathrm{T}}^{||} \right\rangle = 0$ (shown as points). The balance is observed even for events with large A_J. The momentum balance as a function of the distance of particles from the jet axis, ΔR, was investigated as well[2]. Tracks inside jet cones of the size $\Delta R = 0.8$ around the leading and subleading jet axes (middle panel) and tracks outside of these cones (right panel) were used in the study. The in-cone excess towards the leading jet is balanced by the out-of-cone excess in the direction of the subleading jet. The p_{T} difference for dijets is due to low-p_{T} particles ($p_{\mathrm{T}} < 4$ GeV/c) emitted at large angles with respect to the subleading jet axis. These particles are "lost" for the subleading jet reconstruction.

[2] Jet cone radius $\Delta R = \sqrt{\Delta\eta^2 + \Delta\phi^2}$.

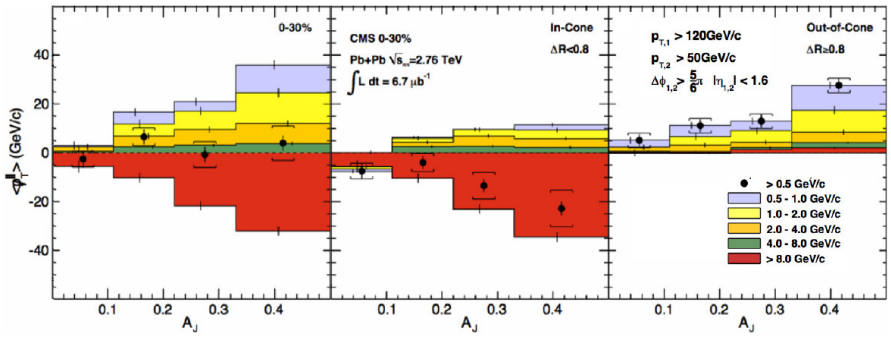

Fig. 4. (Color online) Average missing transverse momentum for the 0–30% central collisions [12]. Tracks with $p_{\mathrm{T}} > 0.5$ GeV/c were used. Bands show the contributions from various ranges of track p_{T}. Points are obtained after summing up all contributions. Left: $\langle \not{p}_{\mathrm{T}}^{||} \rangle$ for all tracks. Middle: $\langle \not{p}_{\mathrm{T}}^{||} \rangle$ for tracks inside ($\Delta R < 0.8$) the leading and subleading jet cones. Right: $\langle \not{p}_{\mathrm{T}}^{||} \rangle$ for tracks outside ($\Delta R > 0.8$) the jet cones.

Fragmentation functions

The experimental observations of jet quenching raise questions concerning the parton energy loss mechanism, such as: do partons first lose energy in the nuclear medium and subsequently fragment as they would do in vacuum, or does the energy loss modify the fragmentation process?

Longitudinal jet fragmentation is commonly studied as a function of a fraction of the parton momentum[3], z, or the parameter $\xi = \ln(1/z) = \ln(p^{\mathrm{jet}}/p_{||}^{\mathrm{track}})$. Fragmentation functions for four centrality bins of PbPb collisions and pp reference data are shown in Fig. 5 (top row). For a direct comparison of PbPb and pp collisions, the deterioration of the jet momentum resolution in PbPb events (caused by large underlying event fluctuations) has to be taken into account. Therefore, the reconstructed p_{T} of every jet in the pp data was smeared, to correct for the difference between the underlying event fluctuations in PbPb and pp collisions. Figure 5 presents the results obtained for jets with $p_{\mathrm{T}} > 100$ GeV/c and tracks with $p_{\mathrm{T}} > 1$ GeV/c reconstructed within the jet cone. The bottom panels show ratios of the PbPb and pp fragmentation functions [14].

The fragmentation function for peripheral PbPb collisions is in good agreement with that for the pp-based reference (leftmost panels in Fig. 5). However, for more central collisions the fragmentation process is modified. In the most central collisions (0–10% centrality bin), there is a strong en-

[3] For experimental data the fraction of the parton's momentum carried by a hadron coming from its fragmentation, z, is calculated as $z = p_{||}^{\mathrm{track}}/p^{\mathrm{jet}}$, where p^{jet} is the jet momentum and $p_{||}^{\mathrm{track}}$ is the projection of track momentum onto the jet axis.

hancement of particles at large ξ (corresponding to low p_{T}), in the mid-ξ region a slight depletion is observed and only in the region of small ξ (where particles have high p_{T}) jet fragmentation in PbPb and pp collisions is similar.

The information obtained from this study is complementary to results of the analyzes of leading hadron and jet R_{AA} and dijet imbalance.

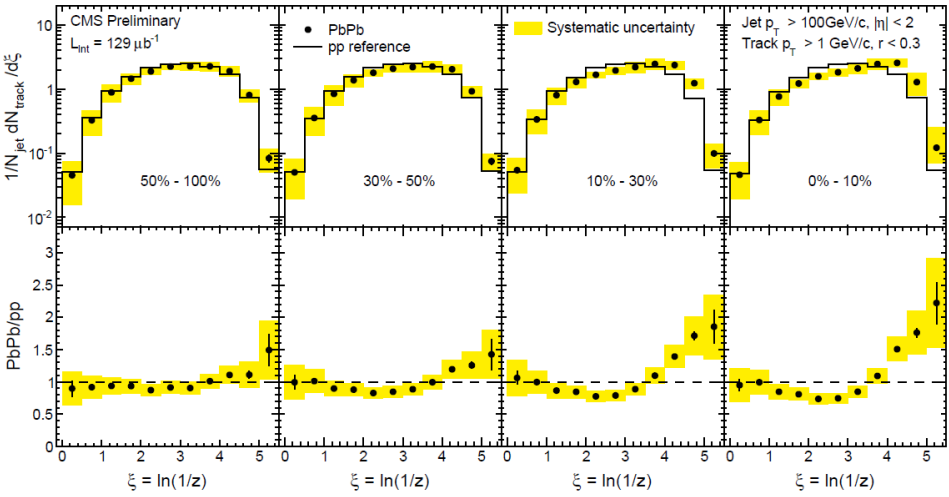

Fig. 5. (Color online) Top row: Jet fragmentation functions for PbPb collisions (solid points) and for the pp reference (histograms) in four centrality classes; jets with $p_{\mathrm{T}} > 100$ GeV/c and tracks with $p_{\mathrm{T}} > 1$ GeV/c were used. Bottom row: Ratios of each PbPb fragmentation function and the corresponding pp reference. Error bars and yellow boxes represent statistical and systematic uncertainties, respectively.

2.2. Quarkonia suppression

The next signature of QGP is the suppression of quarkonium states [15]. In QGP, the constituents of quarkonium state, a heavy quark (Q) and its antiquark ($\bar{Q}$), are thought to be screened by the color charges of the surrounding light quarks and gluons — the Debye screening. Due to the color screening, quarkonia should "melt" and become less abundant. Since various quarkonium states have different binding energies and radii, their dissociation temperatures are different. Hence the spectral analysis of in-medium quarkonia dissociation should provide a QGP thermometer [16].

Before the first measurements from the LHC, the melting picture was experimentally tested only for the charmonium ($c\bar{c}$) family. At lower energies, bottomonium ($b\bar{b}$) states were not accessible due to low cross sections and/or problems with distinguishing different states. The CMS experiment studied both the charmonium family (J/ψ, ψ(2S)) and bottomonia (Υ(1S,

2S, 3S)). A good illustration of the excellent capabilities of CMS is the plot presented in Fig. 6 (left panel), showing the Υ(1S), Υ(2S) and Υ(3S) mass peaks in the $\mu^+\mu^-$ invariant mass distribution for minimum bias PbPb and pp collisions. The Υ(1S) yields are normalized between the two systems. In PbPb collisions, the excited Υ states are suppressed with respect to pp events. The sequential suppression of these three $\Upsilon(n\mathrm{S})$ states in the order of their binding energies is apparent, in agreement with expectations for their dissolution in a hot QCD medium. The suppression is stronger for more loosely bound states, thus Υ(3S) is the most suppressed state of the three studied ones. Bottomonia suppression depends also on collision centrality, as the yields of Υ(1S) and Υ(2S) states were found to decrease for more central PbPb collisions [18].

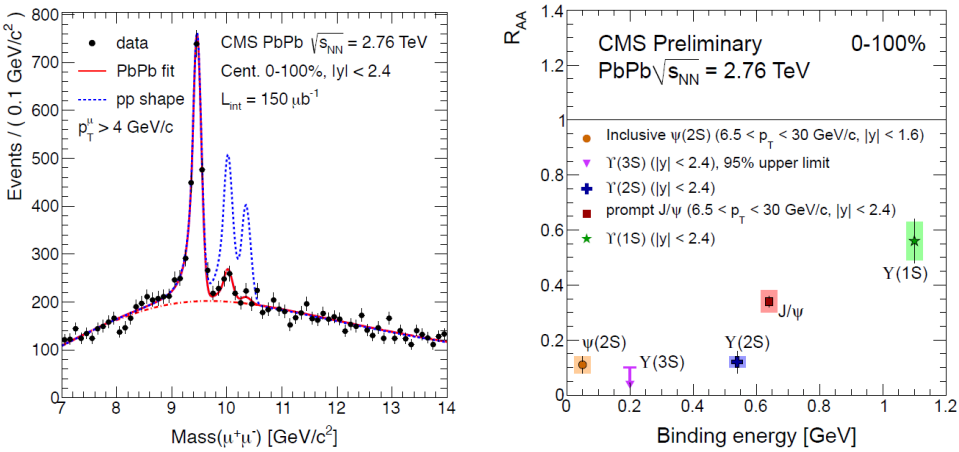

Fig. 6. (Color online) Left: Dimuon invariant-mass distribution in the Υ mass region. The solid (red) line shows the fit to the minimum bias PbPb data. The dashed (blue) line is the fit to the spectrum in pp collisions, normalized to the Υ(1S) peak in PbPb. Right: Minimum bias R_{AA} for all quarkonia measured by CMS (high-p_{T} states of prompt J/ψ [9] and inclusive ψ(2S) [17], as well as Υ(1S, 2S, 3S) states [18]).

One of the goals in these studies is to use the dependence of the observed suppression of various quarkonium states on their binding energies to constrain initial medium properties, *e.g.* the initial temperature. Figure 6 (right panel) shows the nuclear modification factor, R_{AA}, for the charmonium [9, 17] and bottomonium [18] states in minimum bias PbPb collisions as a function of the binding energy[4]. Since Υ(1S) is the most tightly bound state among all quarkonia, it is expected to be the one with the highest dissociation temperature, while ψ(2S), with the smallest binding energy, to

[4] For Υ(3S), the upper limit (95% C.L.) is shown.

be the one with the lowest dissociation temperature and hence the first to melt. The ordering of the suppression is indeed observed and, qualitatively, the sequential melting scenario for quarkonia is confirmed. For quantitative statements, further studies have to be done, in which the effects of the p_{T}-cuts and feed-down contributions have to be evaluated.

Competing effects with opposite contributions, both in the initial and in the final state of the collision, may complicate interpretation of any quarkonia measurement. Quarkonia yields can decrease in PbPb collisions, compared to *pp* collisions, due to initial and final-state effects, but can also increase via a statistical recombination of the partons from quarkonium states which have earlier melted. It is also important to understand effects related to the cold nuclear matter, which can be studied in *p*Pb collisions at the LHC.

3. First *p*Pb results

As it was already mentioned in Introduction, a short run of *p*Pb collisions at $\sqrt{s_{NN}} = 5.02$ TeV took place in September 2012, in preparation for the longer run planned for the beginning of 2013. The run delivered about 2 million events, sufficient to perform measurements of some global characteristics and correlations. The CMS Collaboration analyzed two-particle correlations using this data set and the outcome of the study is presented below.

3.1. Two-particle correlations: the ridge effect

A study of particle correlations in high-energy collisions may shed light on the underlying mechanism of particle production, and thus is being extensively pursued in several experiments. Measurements of two-particle correlations were performed using two-dimensional $\Delta\eta$–$\Delta\phi$ correlation functions, where $\Delta\phi$ is the difference in azimuthal angle between the two particles and $\Delta\eta$ is the difference in pseudorapidity. At RHIC, such studies were done for collisions of deuteron–gold (*d*Au) and gold–gold (AuAu) at the center-of-mass energy of 200 GeV [19, 20]. In AuAu collisions, the long-range (large $\Delta\eta$) near-side ($\Delta\phi \approx 0$) correlations were revealed — the so-called "ridge" effect. The effect was also observed by the CMS experiment in PbPb collisions at $\sqrt{s_{NN}} = 2.76$ TeV [21]. Unexpectedly, it appeared in *pp* collisions at 7 TeV as well when a special selection of events with very high multiplicity was used by CMS [22, 23].

The analysis of two-particle correlations in *p*Pb collisions was performed in classes of track multiplicity, $N_{\mathrm{trk}}^{\mathrm{offline}}$, following the procedure established for *pp* interactions [23]. Particle pairs were formed by associating every trigger particle with all other charged particles from the same p_{T} interval as

the trigger particle. The per-trigger-particle associated yield was defined as

$$\frac{1}{N_{\mathrm{trig}}}\frac{d^2N^{\mathrm{pair}}}{d\Delta\eta\, d\Delta\phi} = B(0,0)\,\frac{S(\Delta\eta,\,\Delta\phi)}{B(\Delta\eta,\,\Delta\phi)}\,, \tag{4}$$

where N_{trig} is the number of trigger particles in the event, the signal distribution, $S(\Delta\eta,\,\Delta\phi)$, is the per-trigger-particle yield of particle pairs from the same event

$$S(\Delta\eta,\,\Delta\phi) = \frac{1}{N_{\mathrm{trig}}}\frac{d^2N^{\mathrm{same}}}{d\Delta\eta\, d\Delta\phi}\,, \tag{5}$$

and the background distribution, $B(\Delta\eta,\,\Delta\phi)$, is the per-trigger-particle yield of particle pairs from the mixed events

$$B(\Delta\eta,\,\Delta\phi) = \frac{1}{N_{\mathrm{trig}}}\frac{d^2N^{\mathrm{mix}}}{d\Delta\eta\, d\Delta\phi}\,. \tag{6}$$

The mixed-event background distribution was constructed by pairing the trigger particles in each event with the associated particles from 10 different random events (belonging to the same track multiplicity class). The signal and background distributions were first calculated for each event, and then averaged over all events within the track multiplicity class.

Two-dimensional two-particle correlation functions for pPb collisions, calculated for pairs of charged particles with $1 < p_{\mathrm{T}} < 3$ GeV/c, are presented in Fig. 7 [24]. For the low-multiplicity selection ($N_{\mathrm{trk}}^{\mathrm{offline}} < 35$), dominant features are the correlation peak near $(\Delta\eta,\,\Delta\phi) = (0,\,0)$, containing

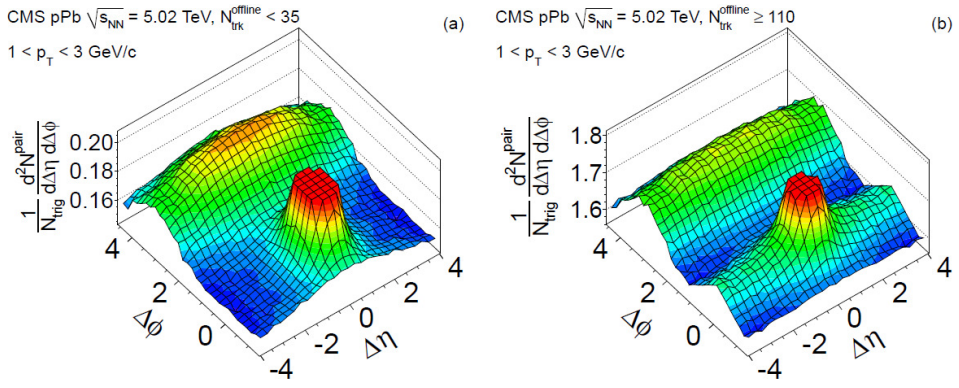

Fig. 7. Two-dimensional (2D) two-particle correlation functions for pairs of charged particles with $1 < p_{\mathrm{T}} < 3$ GeV/c [24]. Results are shown (a) for low-multiplicity events ($N_{\mathrm{trk}}^{\mathrm{offline}} < 35$) and (b) for a high-multiplicity selection ($N_{\mathrm{trk}}^{\mathrm{offline}} \geq 110$). The sharp near-side peaks from jet correlations have been truncated to better illustrate the structure outside that region.

mostly pairs of particles originating from the same jet, and the elongated in $\Delta\eta$ structure at $\Delta\phi \approx \pi$, for pairs of particles coming from back-to-back jets. Particles from resonance decays contribute to these correlations as well. High-multiplicity events ($N_{\mathrm{trk}}^{\mathrm{offline}} \geq 110$), corresponding to central pPb collisions, also show the same-side jet-peak and the back-to-back correlation structure. However, in addition, a pronounced "ridge"-like structure emerges at $\Delta\phi \approx 0$, which extends over at least 4 units of pseudorapidity — the long-range near-side correlations. This is the first observation of such correlations in proton–nucleus collisions.

The strength of the long-range near-side correlations can be further quantified by averaging over $2 < |\Delta\eta| < 4$ and, then, integrating over $|\Delta\phi| < 1.2$. The resulting integrated "ridge yield" is plotted in Fig. 8 as a function of particle p_{T} and event multiplicity, for pp and pPb data. Figure 8 (a) shows that for events with $N_{\mathrm{trk}}^{\mathrm{offline}} \geq 110$ the ridge effect is most apparent in the intermediate transverse momentum range ($1 < p_{\mathrm{T}} < 2$ GeV/c). The multiplicity dependence of the ridge yield for this p_{T} range is presented in Fig. 8 (b). An approximately linear increase with charged particle multiplicity for high-multiplicity events is observed. While the multiplicity and p_{T} dependences of the ridge effect in pPb collisions are qualitatively similar to those seen in pp data at $\sqrt{s} = 7$ TeV, the absolute ridge yield in pPb is significantly larger than in pp collisions of the same particle multiplicity.

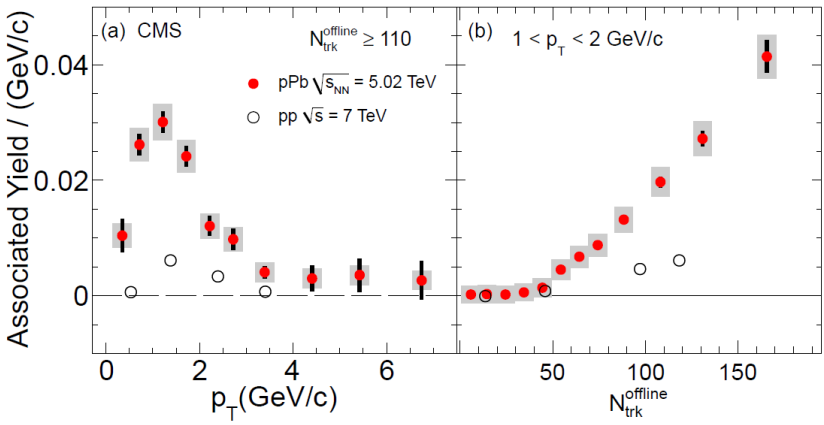

Fig. 8. Associated yield for the near-side of the correlation function averaged over $2 < |\Delta\eta| < 4$ and integrated over $|\Delta\phi| < 1.2$, for 7 TeV pp and 5.02 TeV pPb collisions [24]. (a) The associated yield as a function of p_{T} for events with $N_{\mathrm{trk}}^{\mathrm{offline}} \geq 110$. (b) The associated yield for particles with $1 < p_{\mathrm{T}} < 2$ GeV/c as a function of multiplicity $N_{\mathrm{trk}}^{\mathrm{offline}}$. The p_{T} selection applies to both particles in each pair. Error bars and shaded boxes correspond to statistical and systematic uncertainties, respectively.

Various theoretical models have been proposed to explain the origin of the ridge effect, see Ref. [25] for a recent review. Long-range correlations in pPb collisions were quantitatively predicted in models assuming a collective hydrodynamic expansion of a system with fluctuating initial conditions. The ridge-like structure in pPb collisions was also predicted to arise from initial state gluon correlations in the color-glass condensate (CGC) framework. The CMS experiment has measured the long-range near-side correlations in pPb collisions but also in pp interactions, and a simultaneous description of both these systems should provide constraints on models of the underlying physics processes. With such an improved understanding of the smaller systems, the comparison with PbPb collisions, measured by CMS as well, should provide further insights in understanding of the ridge-like correlations.

4. Summary and outlook

The CMS experiment has a very broad heavy-ion program. The apparatus of CMS allows to investigate various hard probes, as well as bulk particle production and collective phenomena. The presented analyzes, performed for PbPb, pPb and pp collisions collected in the years 2010–2012, are focused on effects of energy loss of partons, dissociation of quarkonium states in the produced strongly-interacting medium and on long-range two-particle correlations. Main findings are specified below.

— The medium created in PbPb collisions at $\sqrt{s_{NN}} = 2.76$ TeV does not quench high-p_{T} photons, Z and W. These unsuppressed probes provide a reference for suppression studies of strongly-interacting probes.

— The suppression of partons was analyzed via measurements of the nuclear modification factor R_{AA} for charged hadrons, jets and non-prompt J/ψ mesons. $R_{AA} < 1$ has been found for these strongly-interacting probes, confirming the presence of jet quenching.

— Further evidence for the jet-quenching effect comes from the analysis of jet–jet and γ-jet events. The transverse-momentum imbalance of dijet events was studied in detail, indicating a strong parton energy loss in the medium and no significant angular decorrelation of the jets. The momentum imbalance of jets is compensated by low-p_{T} particles emitted at large angles with respect to the jet axis. The analysis of photon–jet events also supports the jet-quenching picture.

— For central PbPb collisions, for which large parton energy losses are present, modifications of the jet fragmentation properties have been observed. Fragmentation functions of jets in PbPb, in comparison to pp collisions, show an excess of particles at low p_{T} and no modification at high p_{T}.

— Measurements of R_{AA} of the charmonia and the $\Upsilon(n\mathrm{S})$ states confirm the suppression pattern expected from Debye screening in the hot colored medium — the sequential quarkonia suppression.

— The first analysis of the low-statistics pilot pPb data at 5.02 TeV, on two-particle correlations, has been performed. The ridge effect in high-multiplicity pPb collisions is significantly stronger than that measured in 7 TeV pp collisions of the same particle multiplicity.

Here, only selected results from the CMS experiment were discussed, a complete collection of all submitted CMS heavy-ion publications, as well as a documentation of all preliminary results, can be found in [26].

In early 2013, the LHC accelerator ran in the pPb mode at the energy $\sqrt{s_{NN}} = 5.02$ TeV and in the pp mode at $\sqrt{s} = 2.76$ TeV. The total integrated luminosity recorded by the CMS experiment is 31 nb^{-1} and 5.4 pb^{-1}, for pPb and pp collisions, respectively. With this high-statistics pPb data sample detailed analyzes of possible cold nuclear matter effects could be performed. The pp data set is needed to improve the reference measurements for PbPb collisions.

REFERENCES

[1] S. Chatrchyan *et al.* [CMS Collaboration], *JINST* **03**, S08004 (2008).

[2] M. Gyulassy, M. Plumer, *Phys. Lett.* **B243**, 432 (1990).

[3] J. Adams *et al.* [STAR Collaboration], *Phys. Rev. Lett.* **91**, 072304 (2003).

[4] J. Adams *et al.* [STAR Collaboration], *Phys. Rev. Lett.* **97**, 162301 (2006).

[5] S. Chatrchyan *et al.* [CMS Collaboration], *Phys. Lett.* **B710**, 256 (2012).

[6] CMS Collaboration, Physics Analysis Summary CMS-PAS-HIN-12-008, 2012, `http://cdsweb.cern.ch/record/1472723`

[7] S. Chatrchyan *et al.* [CMS Collaboration], *Phys. Lett.* **B715**, 66 (2012).

[8] S. Chatrchyan *et al.* [CMS Collaboration], *Eur. Phys. J.* **C72**, 1945 (2012).

[9] CMS Collaboration, Physics Analysis Summary CMS-PAS-HIN-12-014, 2012, `http://cdsweb.cern.ch/record/1472735`

[10] CMS Collaboration, Physics Analysis Summary CMS-PAS-HIN-12-004, 2012, `http://cdsweb.cern.ch/record/1472722`

[11] S. Chatrchyan *et al.* [CMS Collaboration], *Phys. Lett.* **B712**, 176 (2012).

[12] S. Chatrchyan *et al.* [CMS Collaboration], *Phys. Rev.* **C84**, 024906 (2011).

[13] S. Chatrchyan *et al.* [CMS Collaboration], *Phys. Lett.* **B718**, 773 (2013).

[14] CMS Collaboration, Physics Analysis Summary CMS-PAS-HIN-12-013, 2012, `http://cdsweb.cern.ch/record/1472734`

[15] T. Matsui, H. Satz, *Phys. Lett.* **B178**, 416 (1986).

[16] S. Digal, P. Petreczky, H. Satz, *Phys. Rev.* **D64**, 094015 (2001).

[17] CMS Collaboration, Physics Analysis Summary CMS-PAS-HIN-12-007, 2012, http://cdsweb.cern.ch/record/1455477

[18] S. Chatrchyan *et al.* [CMS Collaboration], *Phys. Rev. Lett.* **109**, 222301 (2012).

[19] B. Abelev *et al.* [STAR Collaboration], *Phys. Rev.* **C80**, 064912 (2009).

[20] B. Alver *et al.* [PHOBOS Collaboration], *Phys. Rev. Lett.* **104**, 062301 (2010).

[21] S. Chatrchyan *et al.* [CMS Collaboration], *Eur. Phys. J.* **C72**, 2012 (2012).

[22] S. Chatrchyan *et al.* [CMS Collaboration], *J. High Energy Phys.* **09**, 091 (2010).

[23] S. Chatrchyan *et al.* [CMS Collaboration], *J. High Energy Phys.* **07**, 076 (2011).

[24] S. Chatrchyan *et al.* [CMS Collaboration], *Phys. Lett.* **B718**, 795 (2013).

[25] W. Li, *Mod. Phys. Lett.* **A27**, 1230018 (2012).

[26] CMS Collaboration, CMS Public Heavy Ion Results, http://twiki.cern.ch/twiki/bin/view/CMSPublic/PhysicsResultsHIN